Brazilian Journal
of Chemical
Engineering

ISSN 0104-6632
Printed in Brazil
www.abeq.org.br/bjche

Vol. 33, No. 01, pp. 225 - 233, January - March, 2016
dx.doi.org/10.1590/0104-6632.20160331s20140134

AN EXPERIMENTAL STUDY OF H_2 AND CO_2 ADSORPTION BEHAVIOR OF C-MOF-5 AND T-MOF-5: A COMPLEMENTARY STUDY

M. Arjmandi* and M. Pakizeh*

Department of Chemical Engineering, Faculty of Engineering, Ferdowsi University of Mashhad, Mashhad, Iran.
*E-mail: Mehrzad.Arjmandi89@gmail.com; Pakizeh@um.ac.ir

(Submitted: October 28, 2014 ; Revised: April 4, 2015 ; Accepted: April 21, 2015)

Abstract - In this paper the cubic and tetragonal structure of MOF-5 were successfully synthesized and characterized by TGA and SEM analysis. Equilibrium adsorption isotherms of C-MOF-5 and T-MOF-5 for H_2 and CO_2 were measured up to 25 bar at 298 K using a volumetric method. The C-MOF-5 adsorbent synthesized in this study had a 0.107 and 79.9 wt% adsorption capacities at 298 K and 25 bar for H_2 and CO_2, respectively. T-MOF-5 had a H_2 adsorption capacity of 0.122 wt% and CO_2 adsorption capacity of 67.6 wt% at 298 K and 25 bar. This behavior was attributed to more ZnO units in the T-MOF-5 structure. The difference between H_2 and CO_2 adsorption capacity for the cubic and tetragonal structure of MOF-5, suggests that C-MOF-5 and T-MOF-5 are potential adsorbents for the separation of CO_2 and H_2 from gas mixtures, respectively. Langmuir, Freundlich and Sips isotherm models were used to correlate the adsorption isotherms. The results showed that, at 298 K, the fit of the Sips isotherm to the experimental datawas better than Langmuir and Freundlich isotherms. According to TGA results, the thermal decomposition of C-MOF-5 requires a higher temperature than T-MOF-5.
Keywords: Adsorption; Hydrogen; Carbon dioxide; MOF-5; ZnO.

INTRODUCTION

In the last decades, there has been an increasing interest in developing gas storage systems for different applications such as H_2 storage or CO_2 capture (Marco-Lozar *et al.*, 2012; Saha and Deng, 2009; Saha *et al*., 2009; Lou *et al*., 2014).

H_2 is important as a new source of energy for automotive applications. The main challenge in developing this technology is H_2 storage. The development of high H_2 storage capacity materials and safe transportation methods are recognized as requirements for the realization of a H_2 economy. Also, CO_2 emissions resulting from the burning of fossil fuels in ground transportation (cars, public/goods transport vehicles) are among the pressing global environmental problems (Lee *et al*., 2006).

Metal–organic frameworks (MOFs), also known as coordination polymers, are ideal crystalline substances for catalysis and gas separation and storage (Kurmoo *et al.*, 2005; Zheng *et al*., 2006). In addition MOFs generally have high internal surface area and, due to the presence of organic linkers and metal ligands, it is possible to tune their pore size and volume (Mishra *et al*., 2012).

One of the most important MOFs is the $Zn_4O_{13}C_{24}H_{12}$ framework called MOF-5, which was first synthesized in 1999 (Li *et al*., 1999). This framework has potential applications for H_2 storage, CO_2 capture and catalysts (Eddaoudi *et al*., 2002). MOF-5 consists of Zn_4O as metal clusters connected by 1,4-benzenedicarboxylate (BDC) as a linkers to form a porous $Zn_4O(BDC)_3$ framework (Li *et al*., 1999). It has been recognized that MOF-5 occupies either

*To whom correspondence should be addressed

cubic (C-MOF-5) or tetragonal (T-MOF-5) structures (Li *et al*., 1999; Hafizovic *et al*., 2007; Kaye *et al*., 2007; Huang *et al*., 2003).

Zhang and Hu (2011) showed that the composition of cubic and tetragonal MOF-5 calculated with the formulas of $Zn_{4.28}O_{12.8}C_{24}H_{11.3}$ and $Zn_4O_{13}C_{24}H_{12.6}(ZnO)_{1.59}(H_2O)_{1.74}$ respectively. They indicated that the formula of the C-MOF-5 sample was consistent with the stoichiometric formula of novel MOF-5 ($Zn_4O_{13}C_{24}H_{12}$) and the formula of the T-MOF-5 sample was very different from the stoichiometrical formula of novel MOF-5, owing tothe presence of ZnO and H_2O.

Arjmandi and Pakizeh (2013) showed that T-MOF-5 had lower surface area, lower porosity, smaller and more uniform pore size, and more ZnO units compared with C-MOF-5.

Sarmiento-Perez *et al*. (2012) used the Grand Canonical Monte Carlo (GCMC) simulation of CO_2 adsorption on MOF-5 and found the surprising role of the BDC organic ligand in this process. They reported that the organic ligands (BDC) have an important role in CO_2 adsorption on MOF-5.

Skoulidas and Sholl (2005) applied the equilibrium molecular dynamics (EMD) and GCMC to calculate the diffusion and adsorption of CH_4, CO_2, N_2, and H_2 in C-MOF-5. They reported that at low pressure (1-2 bar), a significant increase in CH_4, CO_2, N_2, and H_2 adsorption was not observed and at high pressure (6-7 bar), only CO_2 adsorption was increased.

Spencer *et al*. (2005) used neutron powder diffraction to determine the H_2 adsorption sites in the MOF-5 structure. They reported that the ZnO cluster was primarily responsible for H_2 adsorption while the organic ligand (BDC) played only a secondary role.

Arjmandi and Pakizeh (2014) synthesized and characterized (by XRD, FTIR, N_2 adsorption technique at 77 K and particle size analysis) C-MOF-5 and incorporated it in polyetherimide (PEI) as filler to make C-MOF-5/PEI MMMs and study the effect of C-MOF-5 on CH_4, CO_2, N_2, and H_2 gas permeation through the MMMs. The results showed that C-MOF-5 nanocrystals have the potential (as filler in C-MOF-5/PEI MMMs) to enhance CO_2 separation from H_2, CH_4 and N_2.

Arjmandi *et al*. (2014) investigated the effect of more ZnO units in T-MOF-5 than in the C-MOF-5 structure on the gas permeation properties of T-MOF-5/PEI MMMs. For this purpose, T-MOF-5 was successfully synthesized and carefully characterized by XRD, FTIR, SEM and the N_2 adsorption technique at 77 K. The results showed that T-MOF-5 nanocrystals have the potential (as filler in MMMs) to enhance H_2 separation from CO_2, CH_4 and N_2.

Table 1 summarizes the pore textural property of C-MOF-5 and T-MOF-5 according to our previous studies.

In the present work, to estimate the amount of ZnO in T-MOF-5 compared to C-MOF-5, thermogravimetric analysis (TGA) was performed. To study the effect of more ZnO in the structure of T-MOF-5, the excess adsorption measurements (by the volumetric method) of H_2 and CO_2 on C-MOF-5 and T-MOF-5 were studied at 298 K up to 25 bar. The two samples were characterized for their topology by scanning electron microscopy (SEM) imaging.

EXPERIMENTAL

Synthesis of Adsorbents

The cubic and tetragonal forms of MOF-5 were synthesized based on previously reported procedures (Kaye *et al*., 2007; Huang *et al*., 2003). All chemicals used in this study were obtained from Sigma-Aldrich.

For the synthesis of C-MOF-5, 0.45 g of $Zn(NO_3)_2{\cdot}6H_2O$ (>98%) and 0.083 g of H_2BDC (>99%) were dissolved in a100 mL bottle containing 49 mL of DMF (99.8%) and 1 mL of H_2O. After heating the solution at 70 °C under vigorous stirring, it was placed in an oven at 100 °C for 15 h. The reaction flask was then cooled down to 25 °C. After removing the solvent, the white powder was washed six times with 60 mL of anhydrous DMF and six times with 60 mL of anhydrous CH_2Cl_2 (>99.8%) (each time 10 h), respectively. Finally, the C-MOF-5 crystals were dried at 125 °C for 24 h under vacuum. A schematic representation of the synthesis of C-MOF-5 is summarized in Figure 1.

For the synthesis of T-MOF-5, 1.19 g of $Zn(NO_3)_2{\cdot}6H_2O$ (>98%) and 0.34 g of H_2BDC (>99%) were dissolved in 40 mL of DMF (99.8%) at room temperature. After adding three drops of aqueous H_2O_2 solution, 2.3 mL of triethylamine (TEA, >99.5%) was added dropwise to the reaction flask under strong agitation at 70 °C for 2 h. After placing the flask in an oven at 100 °C for 15 h, it was removed from the oven and cooled down to 25 °C. The white solid obtained was filtered and washed with DMF three times. Finally, the T-MOF-5 was dried at 125 °C for 24 h under vacuum. A schematic of the synthesis of T-MOF-5 is summarized in Figure 2.

Table 1: Pore textural properties of C-MOF-5 and T-MOF-5 samples.

Species	BET specific surface area (m^2/g)	Pore diameter (Å)	Pore volume (cm^3/g)	Ref.
C-MOF-5	2387	8.67	0.99	Arjmandi and Pakizeh (2014)
T-MOF-5	1280	6.30	0.58	Arjmandi *et al*. (2014)

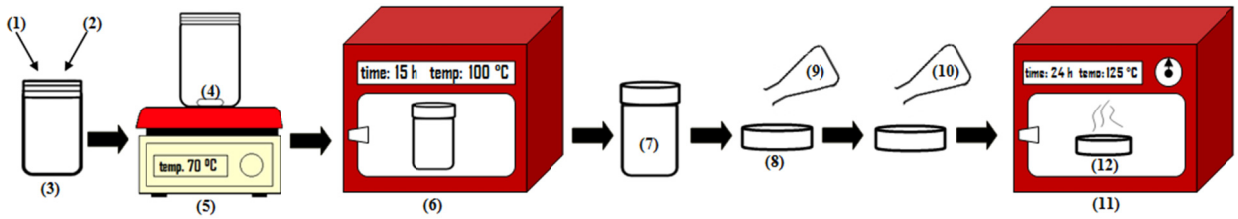

Figure 1: Synthesis of C-MOF-5; (1) $Zn(NO_3)_2{\cdot}6H_2O$, (2) H_2BDC, (3) DMF + H_2O, (4) Magnetic stir bar, (5) Magnetic hotplate, (6) Oven, (7) Reaction flask at 25 °C (with powder + solution), (8) Petri dish, (9) DMF, (10) CH_2CL_2, (11) Vacuum oven, (12) C-MOF-5 powder in a Petri dish with a porous lid.

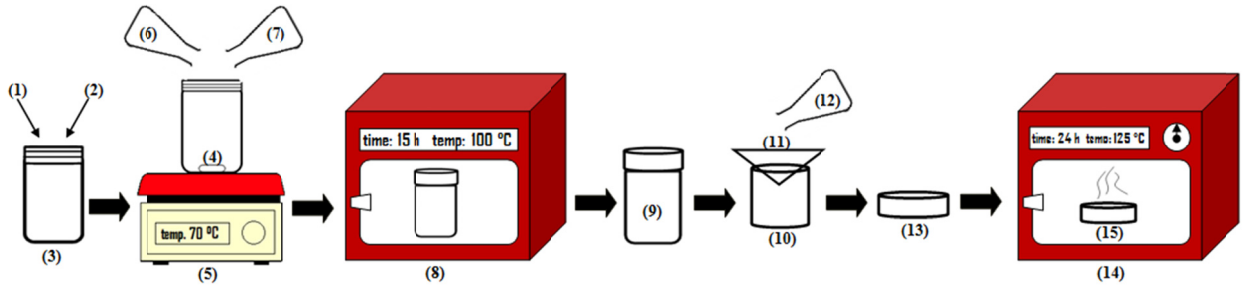

Figure 2: Synthesis of T-MOF-5; (1) $Zn(NO_3)_2{\cdot}6H_2O$, (2) H_2BDC, (3) DMF, (4) Magnetic stir bar, (5) Magnetic hotplate, (6) H_2O_2, (7) TEA, (8) Oven, (9) Reaction flask at 25 °C (with powder + solution), (10) Dish, (11) Filter paper, (12) DMF, (13) Petri dish containing powder, (14) Vacuum oven, (15) T-MOF-5 powder in a Petri dish with a porous lid.

Characterization of Adsorbents

As mentioned above, the XRD, FTIR, N_2 adsorption, surface area measurement and pore textural properties of MOF-5 samples/forms were presented in our previous studies (Arjmandi and Pakizeh, 2014; Arjmandi *et al*. 2014). In this article, thermogravimetric analysis (TGA-50 Shimadzu)in a N_2 atmosphere was used to evaluate the amount of ZnO units in T-MOF-5.Scanning electron microscopy (SEM) images of C-MOF-5 and T-MOF-5 were taken using a Cam Scan SEM model KYKYEM3200 microscope.

Gas Sorption Measurements

The H_2 and CO_2 adsorption capacities of C-MOF-5 and T-MOF-5 were determined in the apparatus based on the volumetric method shown in Figure 3.

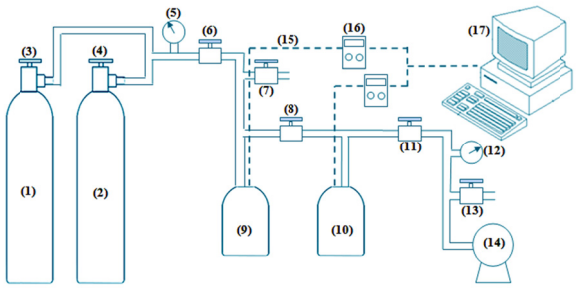

Figure 3: Schematic diagram of the volumetric adsorption apparatus: (1) H_2 gas cylinder, (2) CO_2 gas cylinder, (3) and (4) needle valve, (5) regulator, (6)-(8) needle valve, (9) gas charge cell, (10) adsorption cell, (11) needle valve, (12) regulator, (13) needle valve, (14) vacuum pump, (15) pressure transducer, (16) pressure digital indicator, (17) computer.

The apparatus consisted of two high-pressure stainless steel vessels including the gas charge and adsorption cells (built in-house). The gas charge vessels were connected to a regulator and needle valve (Swagelok, 6DB series) to control the pressure of the gas entering the gas charge cell. Before the sorption process, C-MOF-5 and T-MOF-5 were degassed at 100 °C for about 24 h and the system was evacuated by a vacuum pump (Welch, DuoSeal 1376). Two high precision pressure transducers (Danfoss, MBS 3000 – 2611 – 1 AB04) measured the changes in pressure of the gas and adsorption cell in H_2 and CO_2 adsorption experiments. The H_2 and CO_2 adsorption experiments were conducted at pressures ranging from 0 to 25 bar at ambient temperature.

According to the material balance, the total amount of gas initially available in the gas charge and sorption cells should be equal to the amount of gas in these cells at the steady state plus the amount of gas adsorbed, based on the following equation:

$$\left.\frac{PV}{ZRT}\right|_{c_1} + \left.\frac{PV}{ZRT}\right|_{a_1} = \left.\frac{PV}{ZRT}\right|_{c_2} + \left.\frac{PV}{ZRT}\right|_{a_2} + N_{ads} \qquad (1)$$

where subscripts 1, 2, *c* and *a* denote the initial state, final equilibrium state, gas charge cell and adsorption cell, respectively. Also *V*, *P*, *T*, *R* and N_{ads} represent volume, pressure, temperature, the universal gas constant and amount of gas adsorbed by the adsorbent, respectively. As is evident from Eq. (1), compressibility factors (Z) are required for proper data analysis of the pure gases. The compressibility factors of H_2 and CO_2 were calculated from the Peng-Rabinson (PR) equation of state.

RESULTS AND DISCUSSION

Physical Properties of MOF-5s

The results of thermogravimetric analysis (TGA) are shown in Figure 4 for both tetragonal and cubic MOF-5 nanocrystals. For T-MOF-5, a 15% weight loss occurred in the range of 30–300 °C and then a 43% weight loss, beginning at about 350 ºC. For C-MOF-5, 1.5 and 51.5 wt% weight losses were also observed in the same temperature range of T-MOF-5 weight losses. According to Zhang's experimental results (Zhang and Hu, 2011) it can be said that, for both samples, the first weight loss in TGA corresponds to desorption of water and the second one is associated with the decomposition of MOF-5 to release CO_2 and benzene (Zhang and Hu, 2011). As reported by Zhang and Hu (2011) based on calculation from the chemical formula of novel MOF-5 ($Zn_4O_{13}C_{24}H_{12}$), the weight percent of ZnO units is around 42 wt%. The solid products from the decomposition of both MOF-5s consist of carbon and ZnO (Zhang and Hu, 2011). As shown in Figure 4, the final residual weights of T-MOF-5 and C-MOF-5 were 57 and 48.5 wt%, respectively (regardless of water). For the same amount of carbon in MOF-5s (Zhang and Hu, 2011), the decomposition products of T-MOF-5 contain 8.5 wt% more ZnO than those of C-MOF-5. In addition, C-MOF-5 is more stable than T-MOF-5 because the decomposition temperature of C-MOF-5 is higher than that of T-MOF-5.

Figure 5 shows the scanning electron microscopic images of C-MOF-5 and T-MOF-5 nanocrystals synthesized in this work. The range of particle size of both the C-MOF-5 and T-MOF-5 nanocrystals was 100-150 nm, with no defined morphology. Similar SEM pictures were obtained in literature (Huang *et al*., 2003; Perez *et al*., 2009), with aggregates similar in size (70–100 nm) to the nanocrystals synthesized in this studythat showed no defined crystal morphology.

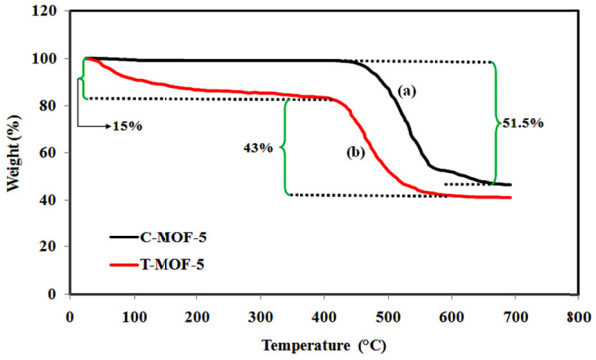

Figure 4: Thermogravimetric curves of (a) C-MOF-5 and (b) T-MOF-5 samples.

Adsorption Equilibrium

The adsorption isotherms of CO_2 and H_2 on both MOF-5s at 298 K and pressures in the range 0–25 bar are plotted in Figures 6 and 7, respectively.

The formula of the C-MOF-5 sample ($Zn_{4.28}O_{12.8}C_{24}H_{11.3}$) is consistent with the stoichiometric formula of novel MOF-5 ($Zn_4O_{13}C_{24}H_{12}$). The comparison of the results for CO_2 and H_2 adsorption on C-MOF-5 in this study with those for CO_2 and H_2 adsorption on novel MOF-5 in the literature (Marco-Lozar *et al*., 2012), indicates the accuracy of the experimental system shown in Figure 3.

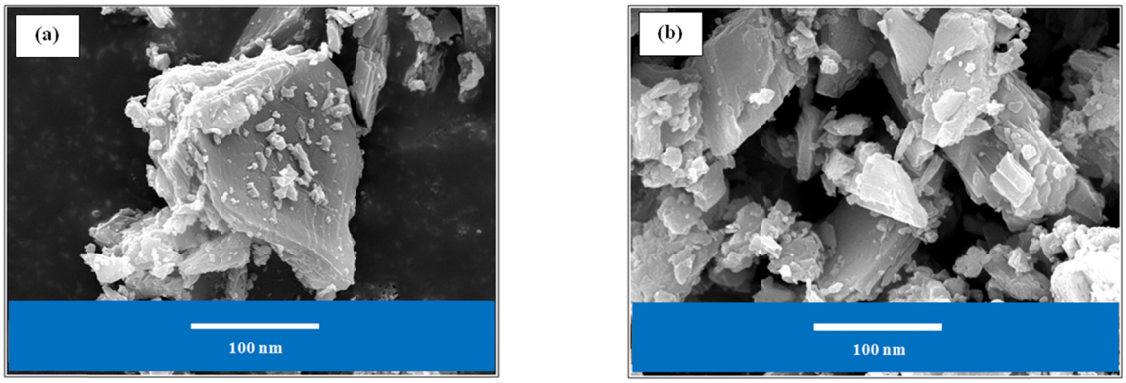

Figure 5: SEM images of (a) C-MOF-5 and (b) T-MOF-5 samples.

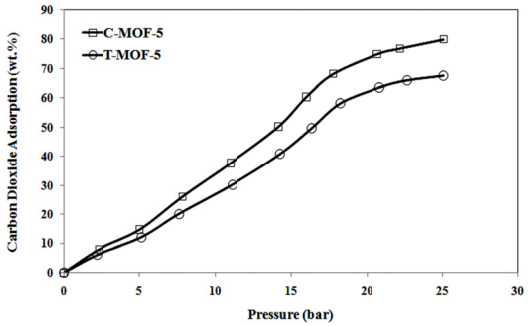

Figure 6: CO_2 adsorption capacity at 298 K and 25 bar of C-MOF-5 and T-MOF-5.

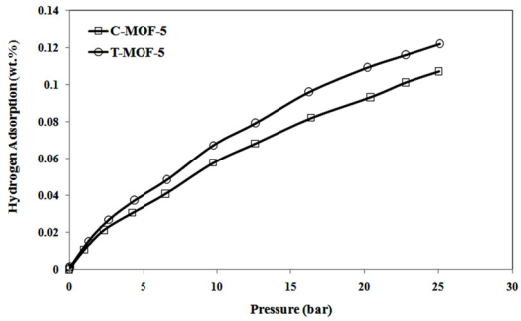

Figure 7: H_2 adsorption capacity at 298 K and 25 bar of C-MOF-5 and T-MOF-5.

According to Figure 6, the adsorption capacity of CO_2 on C-MOF-5 at 298 K and 25 bar is 79.9 wt%, which is about 18% higher than the adsorption capacity of CO_2 on T-MOF-5 at 298 K. In contrast, as shown in Figure 7, T-MOF-5 showed an adsorption capacity of 0.122 wt% for H_2, which is about 12.3% higher than the adsorption capacity of C-MOF-5 for H_2.

For physisorptive materials (such as MOFs) and some gases (such as CH_4), the adsorption capacity has a strong correlation with the surface area and pore volume. For these gases the structure and chemical composition of the adsorbent are not important for the adsorption capacity (Coates, 2000; Zhou, 2010; Anbia *et al*., 2012). In contrast, for H_2 and CO_2 the structure and chemical composition of the adsorbent are important to increase the adsorption capacity.

As noted in the previous sections, the T-MOF-5 nanocrystals have lower surface area, lower porosity and smaller and more uniform pore size than C-MOF-5 nanocrystals.

Also as mentioned earlier, T-MOF-5 contains less CO_2 and organic ligand molecule and more inorganic clusters (containing ZnO units) than C-MOF-5. The difference between the amount of ZnO units in the cubic and tetragonal structures of MOF-5 brings about the difference of H_2 and CO_2 adsorption capacities. Considering that the organic ligand and inorganic clusters in the MOF-5 structure are the major sites of adsorption of CO_2 and H_2, respectively, it can be expected that CO_2 adsorption on T-MOF-5 should be less than that on C-MOF-5. As well, H_2 adsorption on T-MOF-5 is more than that on C-MOF-5.

Accordingly, the higher CO_2 adsorption capacity of C-MOF-5 was attributed to the organic ligand and the higher H_2 adsorption capacity of T-MOF-5 was attributed to the inorganic clusters.

The adsorption selectivities for H_2 and CO_2 were calculated from their adsorption isotherms. The adsorption selectivity of a gas A over gas B was calculated by using Eq. (2) (Lee *et al.*, 2009):

$$\alpha_{A/B} = \left[\frac{V_A}{V_B}\right]_{P,T} \tag{2}$$

where V_A and V_B are the volumes of gases A and B, respectively, adsorbed at any given pressure P and temperature T. The orders of adsorption selectivity for CO_2 and H_2 showed that CO_2/H_2 in T-MOF-5 (553.77) was lower than CO_2/H_2 in C-MOF-5 (746.73).This occurred because there were more adsorption sites for CO_2(organic ligand) in C-MOF-5 than in T-MOF-5 and more H_2 adsorption sites (inorganic clusters) in T-MOF-5 than in C-MOF-5.

Results reported so far in the literature on CO_2 and H_2 adsorption are summarized in Table 2.

Table 2: High-pressure CO_2 and H_2 excess adsorption data at 298 K for selected porous MOFs.

MOFs	BET surface area (m^2/g)	Pressure (bar)	H_2 uptake (wt%)	H_2 uptake (mol/m^3)	CO_2 uptake (wt%)	CO_2 uptake (mol/m^3)	Ref.
MIL-53-Al[a]	-	25	-	-	44.04	10122.52	Bourrelly *et al*. (2005)
MIL-53-Cr[a]	-	25	-	-	44.04	10122.52	Bourrelly *et al*. (2005)
MIL-100[b]	1900	50	-	-	79.27	12596.92	Llewellyn *et al*. (2008)
MIL-101[b]	4230	50	-	-	176.16	17545.71	Llewellyn *et al*. (2008)
MIL-47[a]	-	20	-	-	484.84	11247.25	Bourrelly *et al*. (2005)
MOF-5	2296	35	-	-	95.57	13046.81	Millward and Yaghi (2005)
IRMOF-6	2804	40	-	-	87.20	12866.85	Millward and Yaghi (2005)
MOF-177	4750	42	-	-	147.53	14396.48	Millward and Yaghi (2005)
MIL-100	-	90	0.15	515.91	-	-	Latroche *et al*. (2006)
MIL-101	-	80	0.43	912.76	-	-	Latroche *et al*. (2006)
PCN-10[c]	1407	45	4.2	15973.17	-	-	Wang *et al*. (2008)
PCN-11[c]	1931	45	5.04	18751.12	-	-	Wang *et al*. (2008)
PCN-6	-	50	0.93	-	-	-	Furukawa *et al*. (2007)
HKUST-1	1154	65	0.35	-	-	-	Panella *et al*. (2006)
IRMOF-8	-	30	0.40	1150.86	-	-	Dailly *et al*. (2006)
MOF-5	3800	100[d]	0.57[e]	-	-	-	Kaye *et al*. (2007)
MOF-5[c]	3800	100[d]	7.60	20884.18	-	-	Kaye *et al*. (2007)
IRMOF-8 + Pt/AC	-	100	4.0	-	-	-	Li and Yang (2006)
MOF-5 + Pt/AC	-	100	3.0	-	-	-	Li and Yang (2006)
C-MOF-5	2387	25	0.107	296.71	79.90	10148.63	This study
T-MOF-5	1280	25	0.122	347.38	67.56	8811.51	This study

[a] Measured at 302 K
[b] Measured at 304 K
[a] Measured at 77 K
[c] Absolute pressure
[d] Absolute adsorption

The equilibrium adsorption isotherm is the basis for describing the interaction between adsorbent and adsorbate. In this study, the Langmuir (1916), Freundlich (1906) and Sips (1948) models were used to correlate the adsorption isotherms.

The Langmuir isotherm is written as:

$$q_e = \frac{a_m b p}{1 + bp} \tag{3}$$

where q_e is the H_2 and CO_2 adsorbed amount on MOF-5s, p is the gas pressure, a_m and b are the Langmuir isotherm equation parameters.

The Freundlich isotherm is given by:

$$q_e = k_F p^{1/n} \tag{4}$$

where k_F and n are the Freundlich isotherm equation parameters that can be determined from the experimental H_2 and CO_2 adsorption isotherms.

The Sips isotherm is a combined form of the Langmuir and Freundlich equations deduced for heterogeneous adsorption systems circumventing the limitation of the increasing adsorbate concentration associated with the Freundlich isotherm model. At low adsorbate concentrations, the Sips isotherm reduces to the Freundlich isotherm; while at high concentrations, it predicts a monolayer adsorption capacity characteristic of the Langmuir isotherm. The Sips isotherm is given by:

$$q_e = \frac{k_s p^{\beta}}{1 + \alpha_s p^{\beta}} \tag{5}$$

where k_s, α_s and β are the Sips isotherm constants. These three isotherms were fitted to each of the adsorption data. The adsorption isotherm equation parameters for the Langmuir, Freundlich and Sips equations are listed in Table 3.

Figure 8(a),(b) compares the experimental H_2 and CO_2 adsorption isotherm on the cubic and tetragonal structures of MOF-5 through the Langmuir, Freundlich and Sips isotherms.

It can be seen from these figures that all three isotherm models can reasonably describe the H_2 and CO_2 adsorption isotherms on the two MOF-5 adsorbents, but none of them is accurate enough to predict all isotherms without any error.

The criteria associated with the selection of the best isotherm model were essentially based on the correlation coefficient and R^2. The correlation coefficient shows the fit between experimental data and the isotherm model, while the value of R^2 quantifies the goodness of fit between the experimental data

and calculated data used for plotting the isotherm curves. The results presented in Table 3 show that the Sips isotherm fits better than the Langmuir and Freundlich isotherms at 298 K (especially for CO_2 adsorption on both MOF-5s).

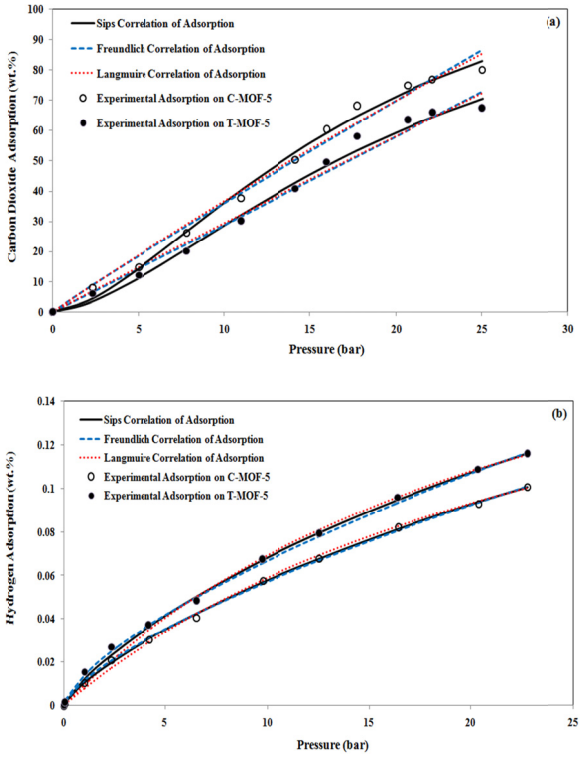

Figure 8: (a) Correlation of CO_2 adsorption isotherm on C-MOF-5 and T-MOF-5 and (b) Correlation of H_2 adsorption isotherm on C-MOF-5 and T-MOF-5 with Langmuir, Freundlich and Sips isotherm models.

Table 3: Summary of adsorption isotherm model parameters for H_2 and CO_2 in C-MOF-5 and T-MOF-5.

Adsorbent	Gas	Isotherm model parameters		
		Langmuir	Freundlich	Sips
C-MOF-5	H_2	a_m= 0.2242 b= 0.0356 R^2= 0.9981	k_F= 0.0114 n= 1.4340 R^2= 0.9992	k_s = 0.0105 α_s = 0.0186 β = 0.7863 R^2= 0.9995
	CO_2	a_m= 712.9 b= 0.0055 R^2= 0.9870	k_F= 3.9780 n= 1.0460 R^2= 0.9854	k_s = 1.1560 α_s = 0.0088 β = 1.6340 R^2= 0.9939
T-MOF-5	H_2	a_m= 0.2441 b= 0.0396 R^2= 0.9981	k_F= 0.0139 n= 1.4720 R^2= 0.9986	k_s = 0.0123 α_s = 0.0272 β = 0.8140 R^2= 0.9993
	CO_2	a_m= 2352 b= 0.0013 R^2= 0.9870	k_F= 2.8 n= 0.9878 R^2= 0.9869	k_s = 0.9186 α_s = 0.0074 β = 1.6080 R^2= 0.9930

CONCLUSIONS

There are two structures of MOF-5: one with the cubic structure (C-MOF-5) and the other tetragonal (T-MOF-5). T-MOF-5 had a lower surface area, lower porosity, smaller and more uniform pore size, and more ZnO units than C-MOF-5. Both the cubic and tetragonal structures of MOF-5 were synthesized and characterized by TGA and SEM and used as adsorbents for H_2 and CO_2 adsorption studies. We found that the CO_2 adsorption capacity of C-MOF-5 at 298 K and 25 bar is greater than that of T-MOF-5, with capacities of 79.9 and 67.5 wt%, respectively. Also we found that the H_2 adsorption capacity of C-MOF-5 at 298 K and 25 bar is less than that of T-MOF-5, with capacities of 0.107 and 0.122 wt%, respectively. This behaviour was attributed to more ZnO units in T-MOF-5 than C-MOF-5. The difference between the H_2 and CO_2 adsorption capacities of T-MOF-5 and C-MOF-5 shows that T-MOF-5 is a better adsorbent for H_2 storage and C-MOF-5 is a better adsorbent for CO_2 capture. The Sips isotherm fit better to the experimental data than the Langmuir and Freundlich isotherms.

Thermal decomposition of T-MOF-5 and C-MOF-5 produced the same products: benzene, CO_2, carbon and ZnO. However, the thermal decomposition of C-MOF-5 required a higher temperature than that of T-MOF-5, indicating that C-MOF-5 is more stable than T-MOF-5.

ACKNOWLEDGEMENT

The authors acknowledge the Iran Nanotechnology Initiative Council for financial support.

REFERENCES

Anbia, M., Hoseini, V., Sheykhi, S., Sorption of methane, hydrogen and carbon dioxide on metal-organic framework, iron terephthalate (MOF-235). Journal of Industrial and Engineering Chemistry, 18, 1149-1152 (2012).

Arjmandi, M., Pakizeh, M., Effects of washing and drying on crystal structure and pore size distribution (PSD) of $Zn_4O_{13}C_{24}H_{12}$ framework (IRMOF-1). Acta Metallurgica Sinica (English Letters), 26, 597-601 (2013).

Arjmandi, M., Pakizeh, M., Mixed matrix membranes incorporated with cubic-MOF-5 for improved Polyetherimide gas separation membranes: Theory and experiment. Journal of

Industrial and Engineering Chemistry, 20, 3857-3868 (2014).

Arjmandi, M., Pakizeh, M., Pirouzram, O., The role of Tetragonal-MOF-5 loadings with extra ZnO molecule on the gas separation performance of mixed matrix membrane. Korean Journal of Chemical Engineering, Accepted (2014).

Bourrelly, S., Llewellyn, P. L., Serre, C., Millange, F., Loiseau, T., Férey, G., Different Adsorption behaviors of methane and carbon dioxide in the isotypic nanoporous metal terephthalates MIL-53 and MIL-47**.** Journal of the American Chemical Society, 127, 13519-13521 (2005).

Coates, J., Interpretation of Infrared Spectra, A Practical Approach. John Wiley and Sons Ltd., New York, 10815 (2000).

Dailly, A., Vajo, J. J., Ahn, C. C., Saturation of hydrogen sorption in Zn benzenedicarboxylate and Zn naphthalenedicarboxylate**.** The Journal of Physical Chemistry, B, 110, 1099-1101 (2006).

Eddaoudi, M., Kim, J., Rosi, N., Vodak, D., Wachter, J., O'Keeffe, M., Yaghi, O. M., Systematic design of pore size and functionality in isoreticular MOFs and their application in methane storage. Science, 295, 469-472 (2002).

Freundlich, H. M. F., Over the adsorption in solution. Journal of Physics and Chemistry, 57(385), e470 (1906).

Furukawa, H., Miller, M. A., Yaghi, O. M., Independent verification of the saturation hydrogen uptake in MOF-177 and establishment of a benchmark for hydrogen adsorption in metal-organic frameworks**.** Journal of Materials Chemistry, 17, 3197-3204 (2007).

Hafizovic, J., Bjorgen, M., Olsbye, U., Dietzel, P. D. C., Bordiga, S., Prestipino, C., Lamberti, C., Lillerud, K. P., The inconsistency in adsorption properties and powder XRD data of MOF-5 is rationalized by framework interpenetration and the presence of organic and inorganic species in the nanocavities**.** Journal of the American Chemical Society, 129, 3612-3620 (2007).

Huang, L., Wang, H., Chen, J., Wang, Z., Sun, J., Zhao, D., Yan, Y., Synthesis, morphology control, and properties of porous metal–organic coordination polymers**.** Microporous and Mesoporous Materials, 58, 105-114 (2003).

Kaye, S. S., Dailly, A., Yaghi, O. M., Long, J. R., Impact of preparation and handling on the hydrogen storage properties of Zn_4O(1,4-benzenedicarboxylate)$_3$ (MOF-5). Journal of the American Chemical Society, 129, 14176-14177 (2007).

Kurmoo, M., Kumagai, H., Chapman, K. W., Kepert, C. J., Reversible ferromagnetic-antiferromagnetic transformation upon dehydration-hydration of the nanoporous coordination framework, $[Co_3(OH)_2(C_4O_4)_2]_{\cdot 3}H_2O$. Chemical Communications, 24, 3012-3014 (2005).

Langmuir, I., The constitution and fundamental properties of solids and liquids. Part I. solids. Journal of the American Chemical Society, 38, 2221-2295 (1916).

Latroche, M., Surblé, S., Serre, C., Mellot-Draznieks, C., Llewellyn, P. L., Lee, J., Chang, J., Jhung, S. H., Férey, G., Hydrogen storage in the giant-pore metal-organic frameworks MIL-100 and MIL-101. Angewandte Chemie International Edition, 45, 8227-8231 (2006).

Lee, J. Y., Wood, C. D., Bradshaw, D., Rosseinsky, M. J., Cooper, A. I., Hydrogen adsorption in microporous hyper cross linked polymers. Chemical Communications, 25, 2670-2672 (2006).

Lee, J. S., Jhung, S. H., Yoon, J. W., Hwang, Y. K., Chang, J. S., Adsorption of methane on porous metal carboxylates. Journal of Industrial and Engineering Chemistry, 15, 674-676 (2009).

Li, H., Eddaoudi, M., O'Keeffe, M., Yaghi, O. M., Design and synthesis of an exceptionally stable and highly porous metal-organic framework. Nature, 402, 276-279 (1999).

Li, Y., Yang, R. T., highly selective asymmetric synthesis of homoallylic amines with and without a .beta.-substituent by the reaction of allylic titanium compounds with chiral imines. Journal of the American Chemical Society, 128, 8136-8137 (2006).

Llewellyn, P. L., Bourrelly, S., Serre, C., Vimont, A., Daturi, M., Hamon, L., Weireld, G. D., Chang, J., Hong, D., Hwang, Y. K., Jhung, S. H., Férey, G., High uptakes of CO_2 and CH_4 in mesoporous metal-organic frameworks MIL-100 and MIL-101. Langmuir, 24, 7245-7250 (2008).

Lou, W., Yang, J., Li, L., Li, J., Adsorption and separation of CO_2 on Fe(II)-MOF-74: Effect of the open metal coordination site. Journal of Solid State Chemistry, 213, 224-228 (2014).

Marco-Lozar, J. P., Juan-Juan, J., Suarez-Garcia, F., Cazorla-Amoros, D., Linares-Solano, A., MOF-5 and activated carbons as adsorbents for gas storage. International Journal of Hydrogen Energy, 37, 2370-2381 (2012).

Millward, A. R., Yaghi, O. M., Metal-organic frameworks with exceptionally high capacity for storage of carbon dioxide at room temperature. Journal of the American Chemical Society, 127, 17998-17999 (2005).

Mishra, P., Mekala, S., Dreisbach, F., Mandal, B.,

Gumma, S., Adsorption of CO_2, CO, CH_4 and N_2 on a zinc based metal organic framework. Separation and Purification Technology, 94, 124-130 (2012).

Panella, B., Hirscher, M., Putter, H., Muller, U., Hydrogen adsorption in metal-organic frameworks: Cu-MOFs and Zn-MOFs Compared. Advanced Functional Materials, 16, 520-524 (2006).

Perez, E. V., Balkus, J. K. J., Ferraris, J. P., Musselman, I. H., Mixed-matrix membranes containing MOF-5 for gas separations. Journal of Membrane Science, 328, 165-173 (2009).

Saha, D., Deng, S., Synthesis, characterization and hydrogen adsorption in mixed crystals of MOF-5 and MOF-177. International Journal of Hydrogen Energy, 34, 2670-2678 (2009).

Saha, D., Wei, Z., Deng, S., Hydrogen adsorption equilibrium and kinetics in metal–organic framework (MOF-5) synthesized with DEF approach. Separation and Purification Technology, 64, 280-287 (2009).

Sarmiento-Perez, R. A., Rodriguez-Albelo, L. M., Gomez, A., Autie-Perez, M., Lewis, D. W., Ruiz-Salvador, A. R., Surprising role of the BDC organic ligand in the adsorption of CO_2 by MOF-5**.** Microporous and Mesoporous Materials, 163, 186-191 (2012).

Sips, R., On the structure of a catalyst surface**.** Journal of Chemical Physics, 16, 490-495 (1948).

Skoulidas, A. I., Sholl, D. S., Self-diffusion and transport diffusion of light gases in metal-organic framework materials assessed using molecular dynamics simulations. Journal of Physical Chemistry, B, 109, 15760-15768 (2005).

Spencer, E. C., Howard, J. A. K., McIntyre, G. J., Rowsell, J. L. C., Yaghi, O. M., Determination of the hydrogen absorption sites in Zn_4O(1,4-benzenedicarboxylate) by single crystal neutron diffraction. Chemical Communications, 3, 278-280 (2006).

Wang, X., Ma, S., Rauch, K., Simmons, J. M., Yuan, D., Wang, X., Yildirim, T., Cole, W. C., López, J. J., Meijere, A., Zhou, H., Metal-organic frameworks based on double-bond-coupled Di-Isophthalate linkers with high hydrogen and methane uptakes. Chemistry of Materials, 20, 3145-3152 (2008).

Zhang, L., Hu, Y. H., Structure distortion of $Zn_4O_{13}C_{24}H_{12}$ framework (MOF-5). Materials Science and Engineering, B, 176, 573-578 (2011).

Zheng, Y., Tong, M., Zhang, W., Chen, X., Assembling magnetic nanowires into network: A layered Co(II)-carboxylate coordination polymer exhibiting the robust single-chain-magnet behavior. Angewandte Chemie International Edition, 45, 6310-6314 (2006).

Zhou, W., Methane storage in porous metal−organic frameworks: Current records and future perspectives. The Chemical Record, 10, 200-204 (2010).